HHS Public Access

Author manuscript

Circ Res. Author manuscript; available in PMC 2016 April 10.

Published in final edited form as:

Circ Res. 2015 April 10; 116(8): 1336–1345. doi:10.1161/CIRCRESAHA.116.304881.

The Mitochondrial Permeability Transition Pore Regulates Endothelial Bioenergetics and Angiogenesis

Raluca Marcu[1,2], **Surya Kotha**[2], **Zhongwei Zhi**[2], **Wan Qin**[2], **Christopher K. Neeley**[1,4], **Ruikang K. Wang**[2,3], **Ying Zheng**[2], and **Brian J. Hawkins**[1]

[1]Mitochondria and Metabolism Center, Department of Anesthesiology and Pain Medicine, University of Washington, Seattle, WA 98109, USA

[2]Department of Bioengineering, University of Washington, Seattle, WA 98109, USA

[3]Department of Ophthalmology, University of Washington, Seattle, WA 98195, USA

[4]General Surgery, University of Michigan, Ann Arbor, USA

Abstract

Rationale—The mitochondrial permeability transition pore (mPTP) is a well-known initiator of cell death that is increasingly recognized as a physiological modulator of cellular metabolism.

Objective—We sought to identify how the genetic deletion of a key regulatory subunit of the mPTP, Cyclophilin D (CypD), influenced endothelial metabolism and intracellular signaling.

Methods and Results—In cultured primary human endothelial cells (ECs), genetic targeting of CypD using siRNA or shRNA resulted in a constitutive increase in mitochondrial matrix Ca^{2+} and NADH. Elevated matrix NADH in turn diminished the cytosolic NAD^+/NADH ratio and triggered a subsequent downregulation of the NAD^+-dependent deacetylase SIRT1. Downstream of SIRT1, CypD-deficient ECs exhibited reduced PTEN expression and a constitutive rise in the phosphorylation of angiogenic Akt. Similar changes in SIRT1, PTEN, and Akt were also noted in the aorta and lungs of CypD KO mice. Functionally, CypD-deficient ECs and aortic tissue from CypD KO mice exhibited a dramatic increase in angiogenesis at baseline and when exposed to vascular endothelial growth factor (VEGF). The NAD^+ precursor Nicotinamide mononucleotide restored the cellular NAD^+/NADH ratio and normalized the CypD-deficient phenotype. CypD KO mice also presented accelerated wound healing and increased neovascularization upon tissue injury as monitored by optical microangiography (OMAG).

Conclusion—Our study reveals the importance of the mPTP in the regulation of endothelial mitochondrial metabolism and vascular function. The mitochondrial regulation of SIRT1 has broad implications in the epigenetic regulation of endothelial phenotype.

Address correspondence to: Dr. Brian J. Hawkins, 850 Republican Street, Seattle, WA 98109-8057, USA, Tel: 206-543-6140, Fax: 206-616-4819, bhawkins@uw.edu, bhawkins@biolifesolutions.com. Dr. Raluca Marcu, 850 Republican Street, Room Brotman 403G, Seattle, WA 98109-8057, USA, Tel: 206-685-4208, Fax: 206-616-4819, rmarcu@uw.edu.

In January 2015, the average time from submission to first decision for all original research papers submitted to *Circulation Research* was 14.7 days.

DISCLOSURES

B.J.H. is currently employed by BioLife Solutions, Bothell, WA.

Keywords

Mitochondria; cyclophilin D; SIRT1; acetylation; NAD^+/NADH ratio; angiogenesis; endothelial function

INTRODUCTION

Once overlooked as merely a passive lining of blood vessels, endothelial cells (ECs) are increasingly recognized as active participants in vascular homeostasis. A particularly important responsibility of the endothelium is to form new blood vessels in a complex and energy-intensive process known as angiogenesis. To fuel angiogenesis, ECs are adept at utilizing glucose as an energy source[1], which allows ECs to proliferate and vascularize hypoxic tissue while preserving oxygen for perivascular cells. Despite a reliance on glycolysis, ECs contain functional mitochondria that are active during angiogenesis[2]. Endothelial mitochondria are therefore considered signaling organelles that modulate the angiogenic process[3] or supply biosynthetic molecules required for growth[4]. Precisely how mitochondrial metabolism impacts endothelial function and angiogenesis is virtually unknown.

An intriguing means to manipulate angiogenesis may involve the mitochondrial permeability transition pore (mPTP). Arsenic-based compounds that target a purported component of the mPTP have an uncanny ability to inhibit endothelial mitochondrial function and angiogenesis in solid tumors[6] and are being developed as anticancer therapies in patients[7]. Pathologically, mPTP activation terminates mitochondrial function and triggers cell death[8]. However, accumulating evidence support a non-lethal role for the mPTP in mitochondrial Ca^{2+} homeostasis, bioenergetics and redox signaling[9]. The mitochondrial matrix protein Cyclophilin D (CypD), which is encoded by the nuclear gene Ppif and inhibited by cyclosporine A (CsA), is a key regulator of Ca^{2+}-induced mPTP opening[10]. Indeed, mitochondria isolated from CypD KO mice have an increased Ca^{2+} retention capacity compared to WT counterparts[11]. As a result, CypD KO mice possess alterations in glucose oxidation that render cardiomyocytes metabolically inflexible and prone to heart failure[12]. CypD KO mice also exhibit changes in branch chain amino acid, pyruvate, and Krebs cycle metabolism[13].

Given that ECs are predominately glycolytic and inherently metabolically inflexible, it is unclear whether the mPTP plays a physiologic role in the vascular intima. Our studies demonstrate a fundamental role for the endothelial mPTP in matrix Ca^{2+} homeostasis and mitochondrial bioenergetics. Genetic CypD targeting in both ECs and mice enhances mitochondrial Ca^{2+} loading and triggers a persistent alteration in cellular NAD^+/NADH homeostasis. Phenotypically, the reduction in the cytosolic NAD^+/NADH ratio reduces SIRT1 expression, which downregulates PTEN and results in constitutive Akt phosphorylation. As a result, both CypD-deficient ECs and CypD KO mice exhibit enhanced angiogenesis in vitro, ex vivo and in vivo upon tissue injury. In total, these findings elucidate a novel pathway by which mitochondrial bioenergetics influence vascular

function, as well as define a Mitochondria-SIRT1 signaling axis that may have broad implications in cell biology.

METHODS

Cell culture

Primary human pulmonary artery endothelial cells (HPAEC) (Invitrogen) were cultured according to the manufacturer's instructions. Human pulmonary microvascular endothelial cells (HPMVEC) were cultured as described previously[14].

Animals

CypD-null and strain-matched controls were obtained from the Jackson Laboratory. All experimental protocols were approved by the University of Washington Institutional Animal Care and Use Committee.

[Ca^{2+}] measurement

Mitochondrial [Ca^{2+}] was measured by confocal microscopy using the FRET-based mitochondrial Ca^{2+} indicator Cameleon D3cpv[15] (Addgene 36324). Cytosolic [Ca^{2+}] was measured by fluorescence microscopy using Fura-2 AM (Molecular Probes).

NADH and NAD^+/NADH ratio measurements

Mitochondrial NAD(P)H autofluorescence was measured by fluorescence microscopy with an UV filter. Cytosolic NAD^+/NADH ratio was measured using Peredox[17] (Addgene 32383). Total intracellular NAD^+/NADH ratio was measured using the NAD^+/NADH Quantitation Kit (BioVision) and the EnzyChrom NAD^+/NADH Assay Kit (BioAssay Systems). Lactate and pyruvate concentrations were measured using Lactate and Pyruvate Assay Kits (Cayman Chemical).

Mitochondrial mass, membrane potential and superoxide production

Mitochondrial mass, membrane potential and superoxide were quantified by flow cytometry using MitoTracker Green, tetramethylrhodamine methyl ester (TMRM), 5,5′,6,6′-tetrachloro-1,1′,3,3′-tetraethylbenzimidazolylcarbocyanine iodide (JC-1) and MitoSox Red (Invitrogen).

Cellular respiration

Oxygen consumption rate (OCR) and extracellular acidification rate (ECAR) were measured using the XF24 Analyzer (Seahorse Bioscience).

Invasion assay

HPAECs were seeded on collagen and provided VEGF every 3rd day. After 7 days, the collagen layer was fixed and stained with primary antibodies against CD31 and Ki67. Image stacks (5 μm) were acquired with a LSM510 META Zeiss confocal microscope and endothelial invasion was quantified by CD31 positivity >5 μm from the plane of focus.

Aortic rings angiogenesis assay

Aortic rings embedded in collagen type I matrix were stimulated with 30 or 90 ng/ml VEGF every 3rd day for 9 days, fixed, stained with DAPI and imaged with a Zeiss Axiovert200 fluorescence microscope. The number of primary and secondary sprouts was quantified in a blinded manner.

Ear wound healing assay

Mouse ear pinna was excised using a 0.5 mm biopsy punch and pictures of the wound were taken biweekly to measure wound size. Microvascular changes during wound healing were visualized and quantified by optical microangiography (OMAG)[20].

Statistical analysis

Data are shown as mean ± SEM of 3 or more independent experiments. Statistical significance was assessed using Student's t test or two-way ANOVA test with Tukey post-hoc analysis at $p < 0.05$ *a priori*.

RESULTS

Genetic inhibition of the mPTP increases mitochondrial calcium levels

Genetic targeting of CypD (Ppif) in primary pulmonary artery endothelial cells (HPAECs) did not dramatically alter either the expression of mitochondrial proteins involved in electron transport and antioxidant defense (Figure 1A) or the overall cellular mitochondrial content (Figure 1B). CypD knockdown did however cause an increase in the length and degree of mitochondrial branching as measured by the mitochondrial form factor (Figure 1C, Online Figures IA, IB), a morphological change reflected by a more complex and reticulated mitochondrial network in Ppif siRNA HPAECs (Figure 1D). As the mPTP is a known regulator of mitochondrial matrix Ca^{2+} ($[Ca^{2+}]_m$), ECs were transfected with the FRET-based mitochondrial Ca^{2+} sensor Cameleon D3cpv[15]. CypD knockdown significantly increased $[Ca^{2+}]_m$ at baseline (Figure 1E), suggesting constitutive mPTP activation in ECs similar to that observed in cardiomyocytes[12]. While we anticipated elevated $[Ca^{2+}]_m$ in the presence of Ca^{2+}-mobilizing agonists such as VEGF or histamine, a significant rise in baseline $[Ca^{2+}]_m$ was unexpected given that ECs are non-excitable cells without the excitation-contraction coupling present in cardiomyocytes. Further analysis revealed sporadic Ca^{2+} transients in serum-containing media in the absence of additional agonists (Figure 1F), with similar oscillatory pattern upon Cyp D deletion or mPTP inhibition by CsA (Online Figures IC, ID), which would be sufficient to load Ca^{2+} into mitochondria. Indeed, Cameleon D3cpv $[Ca^{2+}]_m$ measurements revealed similar Ca^{2+} transients in mitochondrial matrix of both control and Ppif siRNA HPAECs in the presence of serum (Online Figure IE). In total, these findings indicate that the mPTP is an important regulator of endothelial mitochondrial Ca^{2+} homeostasis.

CypD influences endothelial mitochondrial functions

The elevated basal $[Ca^{2+}]_m$ in CypD-deficient ECs would likely elicit mitochondrial functional alterations. Indeed, CypD deletion evoked a significant rise in mitochondrial

membrane potential as detected by the cationic fluorescent indicators TMRM (Figure 2A) and JC-1 (Figure 2B). The rise in membrane potential corresponded with elevated basal respiration: 59.95 ± 2.24 pmol/min O_2 for Ppif siRNA ECs compared to 30.98 ± 1.34 pmol/min for control cells (Figure 2C, 2D). Inhibition of ATP synthase by oligomycin lowered OCR to similar levels in both CypD-deficient and control ECs, indicating that the elevation in respiration was coupled to ATP production. However there was no effect of CypD targeting on overall cellular ATP levels in either proliferating or confluent ECs (Figure 2E). Moreover, lactate production (as detected by ECAR) was similar between CypD-deficient and control ECs (Figure 2F), indicating that CypD knockdown did not simply shift energy production from the cytosol to the mitochondria. Rather, this data suggests increased mitochondrial ATP generation paired with ATP consumption, resulting in a net neutral ATP level. Increased endothelial respiration also evoked mitochondrial ROS generation (Figure 2G) that would imply CypD-deficient ECs might be less metabolically robust and more prone to dysfunction and death. Paradoxically, CypD-deficient ECs appear to be better able to respond to increases in energy demand as denoted by a significant increase in spare respiratory capacity (Figure 2H) suggesting that CypD targeting conveys a protective cellular phenotype.

Endothelial mPTP inactivation triggers NADH accumulation and alters cytosolic NAD^+/NADH homeostasis

Mitochondrial Ca^{2+} activates Ca^{2+}-sensitive dehydrogenases that increase NADH production[21] in order to drive respiration. Consistent with the measured increase in $[Ca^{2+}]_m$ and OCR, CypD-deficient ECs exhibited a 27.5 ± 0.032% rise in basal mitochondrial NAD(P)H autofluorescence versus controls (Figure 3A). Recent data from our laboratory has shown that histamine stimulation of ECs results in mitochondrial Ca^{2+} loading and persistent accumulation of NAD(P)H in the matrix[22]. However, histamine stimulation of CypD-deficient ECs did not further increase mitochondrial NAD(P)H (Figure 3B), suggesting that the basal increase in $[Ca^{2+}]_m$ maximally activates the Ca^{2+}-dependent dehydrogenases. Approximately 75% of cellular NAD^+/NADH is localized within mitochondria[23]. As such, direct measurement of total cellular NADH revealed that mPTP inhibition with CsA stimulated NADH production (Online Figure IF) and a reciprocal reduction in the NAD^+/NADH ratio to a similar degree as acute mitochondrial Ca^{2+} loading using histamine (Online Figure IH). No significant changes in NAD^+ levels were detected (Online Figure IG). To recapitulate these results in vivo, the NAD^+/NADH ratio was measured in tissues obtained from CypD KO mice, the mitochondria from which exhibit an enhanced ability to sequester Ca^{2+} (Figure 3C). Similar to ECs, CypD KO mice had a decreased NAD^+/NADH ratio in both the aorta and endothelial-rich lung tissue when assessing total cellular NAD^+ and NADH (Figure 3D). Intraperitoneal injection of nicotinamide mononucleotide (NMN), a cell-permeable NAD^+ precursor, completely restored the NAD^+/NADH ratio in CypD KO mice.

To counter the buildup of NADH within mitochondria, our group recently discovered that matrix reducing equivalents transmit to the cytosol[22]. CsA evoked a significant reduction in the cytosolic NAD^+/NADH ratio ($[NAD^+/NADH]_{cyt}$) as calculated by the cytosolic concentrations of NADH-linked lactate and pyruvate (Figure 3E). Control ECs had a similar

reduction in $[NAD^+/NADH]_{cyt}$ when mitochondria were acutely loaded with Ca^{2+} using histamine. In contrast, CypD-deficient ECs exhibited a significant basal reduction in the $[NAD^+/NADH]_{cyt}$ (28% ± 0.01) that was unaltered by histamine (Figure 3E). To confirm these results, $[NAD^+/NADH]_{cyt}$ was directly measured by confocal microscopy using the genetically encoded ratiometric sensor Peredox[17]. Similar to the lactate/pyruvate measurements, Peredox measurements revealed a significant reduction in the $[NAD^+/NADH]_{cyt}$ from 102 ± 9.2 in scrambled siRNA cells to 77.63 ± 4.9 in Ppif siRNA cells which was normalized in the presence of NMN (Figure 3F, Online Figure I-I). Thus, genetic mPTP inactivation evokes an elevation in $[Ca^{2+}]_m$ that enhances mitochondrial NADH production and alters cellular NAD^+/NADH metabolism.

CypD-mediated $[NAD^+/NADH]_{cyt}$ alterations influence SIRT1 expression

The NAD^+/NADH ratio regulates the activity[24] and expression[25] of the sirtuin family of NAD^+-dependent deacetlyases. CypD KO lung and aortic tissues displayed a significant decrease in the expression of SIRT1 (Figures 4A, 4B) similar to that of CypD-deficient ECs (Figures 4C, 4D). Immortalized human pulmonary microvascular ECs (HPMVECs) in which CypD was targeted using shRNA also exhibited reduced SIRT1 protein levels (Figures 4C, 4D), demonstrating that the CypD-mediated regulation of SIRT1 is not exclusive to the aorta and pulmonary artery. Indeed, follow-up analysis revealed a strong positive correlation between CypD and SIRT1 expression in both HPAECs and HPMVECs (Figure 4E). Pharmacologic inhibition of mitochondrial Ca^{2+} export through the Na^+/Ca^{2+} exchanger (mNCLX) using CGP-37157 also reduced SIRT1 protein levels similar to CypD knockdown (Online Figure IIA), effectively linking SIRT1 expression to $[Ca^{2+}]_m$.

A reduction in SIRT1 expression concomitant with a decrease in NAD^+/NADH ratio would predictably trigger an increase in protein acetylation. Indeed, overall protein acetylation was elevated in both CypD KO aortic and lung tissues (Figures 4F, 4G). No difference in the protein levels of the acetyl transferase CBP was noted between control and CypD-deficient cells (Online Figures IIB, IIC), implying that acetylation was due to diminished deacetylation. SIRT1 expression was restored by NMN supplementation, confirming that SIRT1 levels were responsive to $[NAD^+/NADH]_{cyt}$ (Figure 4H). We hypothesized that SIRT1 regulation in CypD-deficient ECs may be tied to the NAD^+/NADH ratio by the actions of the NADH-sensitive transcription factor CtBP (C-terminal binding protein)[28]. However, we found no significant difference in CtBP expression between control and CypD-deficient ECs (Online Figures IIB, IID), suggesting an alternative mechanism for SIRT1 regulation.

CypD-mediated SIRT1 alterations influence PTEN expression and Akt phosphorylation

Phosphatase and tensin homolog (PTEN) is indispensible for angiogenesis[29] and has been implicated in vascular function in diabetes[30]. SIRT1 regulates PTEN acetylation and enzymatic activity[31], but has no known role in PTEN expression. A reduction in both CypD and SIRT1 corresponded to diminished PTEN expression in ECs (Figure 5A). Inhibition of Ca^{2+} efflux through the mNCLX (CGP-37157) also resulted in decreased PTEN expression (Online Figure IIA), demonstrating that $[Ca^{2+}]_m$ is a key regulator of PTEN protein levels. Normalization of the $[NAD^+/NADH]_{cyt}$ with NMN increased PTEN protein levels in CypD-

deficient ECs (Figure 5B). In addition to expression, PTEN exhibited enhanced acetylation in CypD-deficient ECs (Online Figures IIIA, IIIB) that may further inhibit enzymatic activity. PTEN protein levels were lower in the lung, but not aorta, of CypD KO mice compared with controls (Online Figures IIIC, IIID). While PTEN immunoprecipitation could not be performed in aortic homogenate, CypD KO aortic tissue did exhibit increased acetylation that corresponded to PTEN via western blotting (Online Figure IIIE). Liver tissue obtained from CypD KO mice exhibits an overall increase in acetylation (Online Figure IIIF) similar to the aorta and lung. PTEN immunoprecipitated from CypD KO liver homogenate revealed significant acetylation compared to the WT control (Online Figures IIIG, IIIH). Therefore, genetic inactivation of CypD in ECs and tissues results in PTEN downregulation and/or increased acetylation that would diminish enzyme activity.

Akt is an important downstream target of PTEN that is phosphorylated by numerous agonists such as histamine[32] and VEGF[33]. Consistent with a reduction in PTEN activity and/or expression, CypD genetic knockdown effectively increased Akt phosphorylation in unstimulated HPAECs and HPMVECs (Figure 5A) as well as in aortic and lung tissue from CypD KO mice (Figure 5C). Genetic targeting of SIRT1 by siRNA resulted in significant decrease in PTEN and a coincident increase in Akt phosphorylation that was unresponsive to NMN (Figure 5E). Conversely, PTEN overexpression in CypD-deficient HPAECs reduced basal Akt phosphorylation without altering SIRT1 levels (Figure 5F) [34](Addgene plasmid 10750). Taken together, these findings demonstrate that PTEN is downstream of SIRT1 and its expression is governed by the $[NAD^+/NADH]_{cyt}$ in CypD-deficient ECs. Pharmacologic inhibition of SIRT1 deacetylase activity with nicotinamide also resulted in increased Akt activation (Figure 5D).

CypD deletion increases endothelial proliferation and angiogenesis

CypD-deficient ECs displayed a significant increase in cell number that calculated as 23.4 ± 1.02% reduction in doubling time and was normalized by NMN (Figure 6A). Challenging CypD-deficient HPAECs with VEGF evoked an even further increase in Akt phosphorylation versus controls (Figure 6B), suggesting that CypD targeting may increase the inherent angiogenic potential of ECs. CypD-deficient HPAECs were therefore plated on collagen matrix and endothelial invasion evaluated after 7 days in culture (Figure 6C) both in the absence and presence of VEGF and NMN. Western blotting was used to confirm that CypD expression remained depressed during the time course of the invasion assay (Online Figure IVA). Consistent with decreased doubling time CypD-deficient ECs exhibited an increased invasion frequency both at baseline and in response to VEGF (Figure 6D). NMN strongly reduced endothelial invasion in CypD-deficient but not control ECs, supporting the primacy of the $[NAD^+/NADH]_{cyt}$ in the CypD-deficient phenotype. Further analysis revealed that CypD-deficient ECs experienced deeper basal invasion depth (25.37 ± 0.58 μm SEM, n=278 processes) with early lumen formation versus control ECs (12.3 ± 7.38 μm SEM, n=26 processes) that in many cases colocalized with the proliferation marker Ki-67 (Figure 6C).

Aortas from WT and CypD KO mice were also evaluated for ex vivo vascular remodeling using the aortic ring angiogenesis assay. In response to VEGF (30 ng/ml), CypD KO aortic

rings experienced significantly increased vessel formation (primary sprouts and secondary branches) compared to WT counterparts that was normalized by NMN (Figures 6E–G). NMN did not diminish sprout formation in WT aortas in which vessel formation was induced by elevated VEGF (90 ng/ml) (Online Figure IVB). No differences in VEGF receptor expression were noted between WT and CypD KO aorta and lung tissues (Online Figure IVC), excluding the possibility that CypD KO mice were simply more responsive to agonist stimulation. To recapitulate our findings in vivo, new vessel formation was monitored during tissue injury by optical microangiography (OMAG)[20] during ear wound healing. CypD KO mice showed earlier onset and significantly accelerated wound closure compared to WT counterparts (Figure 7A), which correlated with increased vascular distribution around the wound at 14 days after ear excision (Figure 7B). Angiographic quantitation of vessel area density revealed a significant increase in wound area vessel density in CypD KO animals: 0.218±0.05 KO vs 0.048±0.02 WT (mean ±SEM, n=3) after wounding but not at baseline (Figure 7C). In total, our results support the mitochondrial regulation of angiogenesis through the NAD^+/NADH dependent regulation of SIRT1 and PTEN (Figure 7D).

DISCUSSION

The discovery that CypD KO mice have a propensity for heart failure[12] has accelerated interest in the physiological actions of the mPTP[35]. In the present study, ECs in which the regulatory subunit CypD was genetically targeted exhibited an increase in both membrane potential and matrix Ca^{2+} that are indicative of constitutive low-level mPTP opening. Elevated matrix Ca^{2+} was likely due to the presence of variable Ca^{2+} transients at baseline. Our results therefore support the regulatory role of constitutive mPTP activity in EC Ca^{2+} homeostasis in agreement with documented data in metabolically-active cardiomyocytes[12], hepatocytes[36] and neurons[37].

CypD-deficient ECs exhibited a striking mitochondrial functional phenotype as indicated by increased NADH production and respiration which we attribute to Ca^{2+} stimulation of matrix dehydrogenases[21]. Similar to the heart[38], ECs also appear to exhibit a Ca^{2+}-mediated increase in ATP synthase activity as witnessed by the dramatic reduction in respiration using oligomycin. However, unlike cardiomyocytes where NADH production is effectively paired with consumption, the low energetic requirements of ECs apparently allow mitochondrial NADH production to outpace consumption and accumulate. We noted a similar rise in matrix NADH in response to repetitive Ca^{2+} oscillations[22], further supporting that Ca^{2+} is the driving force behind endothelial mitochondrial NADH accumulation, and a reduction in the cellular and the cytosolic NAD^+/NADH ratios. A similar buildup of matrix NADH and a reduction in the cellular NAD^+/NADH ratio was observed in cardiac tissue in which NADH oxidation was perturbed by genetic deletion of the mitochondrial complex I subunit Ndufs4[39]. As we recently discovered, a buildup of NADH in endothelial mitochondria can transmit to the cytosol, possibly via the reverse activation of the malate-aspartate shuttle[22], which can transmit reducing equivalents from the mitochondria to the cytosol in liver mitochondria[40].

The $[NAD^+/NADH]_{cyt}$ is a key determinant of cytosolic protein acetylation via sirtuins. Both CypD-deficient ECs and CypD KO mice exhibited a significant decline in SIRT1 expression, which is regulated largely by nutrient status and metabolic transcription factors. Our study strengthens the relationship between SIRT1 expression and the $[NAD^+/NADH]_{cyt}$, but is unique in that all experiments were performed under normal nutrient availability. This distinction is important, and reveals that SIRT1 regulation is impacted not only by nutrient availability per se, but also by the mitochondrial integration of Ca^{2+} signals. ECs appear to interpret a chronic Ca^{2+}-stimulated increase in mitochondrial bioenergetics and the resultant reduction in the $[NAD^+/NADH]_{cyt}$ as an imbalance between energy production and energy demand similar to that triggered by nutrient excess and, as a result, repress SIRT1 expression. SIRT1 expression is depressed in diabetic mice[41] and in patients with chronic obstructive pulmonary disease[42]. Based on our findings, it is interesting to speculate whether endothelial mitochondrial bioenergetics may contribute to SIRT1 downregulation and the vascular complications present in these inflammatory-related diseases. In muscle tissue, SIRT1 diminishes the transcription and activity of PGC1-α, which reduces the expression of genes involved in mitochondrial electron transport, transcription, and fatty acid metabolism[43]. However, we detected no changes in PGC1-α protein and mRNA levels and mitochondrial biogenesis markers (Online Figures VA–C), excluding the role of PGC-1α in the CypD endothelial phenotype.

Pharmacologic mPTP blockade protects from ischemia/reperfusion injury by activating pro-survival Akt[44]. Our data support this finding, but also define a linear pathway in which an mPTP-mediated reduction in $[NAD^+/NADH]_{cyt}$ downregulates SIRT1, resulting in PTEN inhibition and Akt phosphorylation. As SIRT1 can directly target Akt, lowered SIRT1 expression would theoretically enhance Akt acetylation and diminish its phosphorylation[45]. In contrast, our study indicates that SIRT1 affects Akt indirectly through PTEN inactivation in ECs. A similar relationship between SIRT1 expression and Akt activation was noted in cancer cells[46] due to an increase in PTEN acetylation. Enhanced oxidant generation can also directly inactivate PTEN by triggering both intramolecular cysteine bonding[47] and S-glutathionylation. While we cannot completely exclude the possibility that CypD-deficient ECs also inhibit PTEN via oxidation, any oxidant-mediated enzymatic inactivation is secondary to the reduction in PTEN expression, as NMN completely normalizes SIRT1 levels, PTEN expression, and Akt phosphorylation in CypD-deficient ECs without influencing oxidant generation (Online Figure VD). This data strongly suggests that it is the NAD^+/NADH ratio-mediated regulation of SIRT1 and PTEN expression, and not the increase in mitochondrial oxidant generation, which ultimately drives the CypD-deficient phenotype.

While incredibly varied in clinical presentation, a common thread among cardiovascular disease patients is endothelial dysfunction and impaired angiogenesis either as a primary pathology or as collateral damage. Previous work indicates a positive interaction between SIRT1 and angiogenesis, as genetic SIRT1 deletion retards vessel growth in vivo[49]. In contrast, our results demonstrate a negative relationship between SIRT1 expression and angiogenesis when genetic CypD targeting only diminishes SIRT1 levels, which is more biologically relevant than complete SIRT1 deletion. CypD KO mice typically do not present with an overt pathology, but rather as a latent phenotype that manifests only in the presence

of an additional stressor[12]. Indeed our in vivo data show increased neovascularization in CypD KO mice following tissue wounding, but no significant vascular phenotype at baseline. Thus, CypD KO animals may more closely mimic the endothelial dysfunction that occurs in humans during the progression of chronic disease. Further investigation is required to determine the therapeutic implications of our findings, and whether CypD-mediated angiogenesis is restricted to oxygenated tissues that can support increased mitochondrial respiration.

Acknowledgments

We thank Seahorse Bioscience for reagents and technical instruction.

SOURCES OF FUNDING

This study was supported by R01HL093140, R01EB009862 to R.K.W., 12SDG9230006, DP2DK102258 to Y.Z., HL094536, UW RRF award to B.J.H..

Nonstandard Abbreviations and Acronyms

CsA	yclosporine A
EC	Endothelial cells
ECAR	Extracellular acidification rate
HPAEC	Human pulmonary artery endothelial cells
HPMVEC	Human pulmonary microvascular endothelial cells
mNCLX	Mitochondrial Na^+/Ca^{2+} exchanger
mPTP	Mitochondrial permeability transition pore
NMN	Nicotinamide mononucleotide
NAM	Nicotinamide
OMAG	Optical microangiography
OCR	Oxygen consumption rate
ROSE	Reactive Oxygen Species
TSA	Trichostatin A
VEGF	Vascular endothelial growth factor

References

1. De Bock K, Georgiadou M, Schoors S, Kuchnio A, Wong BW, Cantelmo AR, Quaegebeur A, Ghesquiere B, Cauwenberghs S, Eelen G, Phng LK, Betz I, Tembuyser B, Brepoels K, Welti J, Geudens I, Segura I, Cruys B, Bifari F, Decimo I, Blanco R, Wyns S, Vangindertael J, Rocha S, Collins RT, Munck S, Daelemans D, Imamura H, Devlieger R, Rider M, Van Veldhoven PP, Schuit F, Bartrons R, Hofkens J, Fraisl P, Telang S, Deberardinis RJ, Schoonjans L, Vinckier S, Chesney J, Gerhardt H, Dewerchin M, Carmeliet P. Role of PFKFB3-Driven Glycolysis in Vessel Sprouting. Cell. 2013; 154:651–63. [PubMed: 23911327]
2. Rohlena J, Dong LF, Kluckova K, Zobalova R, Goodwin J, Tilly D, Stursa J, Pecinova A, Philimonenko A, Hozak P, Banerjee J, Ledvina M, Sen CK, Houstek J, Coster MJ, Neuzil J.

Mitochondrially targeted alpha-tocopheryl succinate is antiangiogenic: potential benefit against tumor angiogenesis but caution against wound healing. Antioxid Redox Signal. 2011; 15:2923–35. [PubMed: 21902599]

3. Davidson SM, Duchen MR. Endothelial mitochondria: contributing to vascular function and disease. Circulation research. 2007; 100:1128–41. [PubMed: 17463328]
4. Eelen G, Cruys B, Welti J, De Bock K, Carmeliet P. Control of vessel sprouting by genetic and metabolic determinants. Trends Endocrinol Metab. 2013
5. Halestrap AP. What is the mitochondrial permeability transition pore? Journal of molecular and cellular cardiology. 2009; 46:821–31. [PubMed: 19265700]
6. Don AS, Kisker O, Dilda P, Donoghue N, Zhao X, Decollogne S, Creighton B, Flynn E, Folkman J, Hogg PJ. A peptide trivalent arsenical inhibits tumor angiogenesis by perturbing mitochondrial function in angiogenic endothelial cells. Cancer Cell. 2003; 3:497–509. [PubMed: 12781367]
7. Dilda PJ, Decollogne S, Weerakoon L, Norris MD, Haber M, Allen JD, Hogg PJ. Optimization of the antitumor efficacy of a synthetic mitochondrial toxin by increasing the residence time in the cytosol. Journal of medicinal chemistry. 2009; 52:6209–16. [PubMed: 19788237]
8. Rasola A, Bernardi P. Mitochondrial permeability transition in Ca(2+)-dependent apoptosis and necrosis. Cell Calcium. 2011; 50:222–33. [PubMed: 21601280]
9. Hom JR, Quintanilla RA, Hoffman DL, de Mesy Bentley KL, Molkentin JD, Sheu SS, Porter GA Jr. The permeability transition pore controls cardiac mitochondrial maturation and myocyte differentiation. Developmental cell. 2011; 21:469–78. [PubMed: 21920313]
10. Baines CP, Kaiser RA, Purcell NH, Blair NS, Osinska H, Hambleton MA, Brunskill EW, Sayen MR, Gottlieb RA, Dorn GW, Robbins J, Molkentin JD. Loss of cyclophilin D reveals a critical role for mitochondrial permeability transition in cell death. Nature. 2005; 434:658–62. [PubMed: 15800627]
11. Basso E, Fante L, Fowlkes J, Petronilli V, Forte MA, Bernardi P. Properties of the permeability transition pore in mitochondria devoid of Cyclophilin D. The Journal of biological chemistry. 2005; 280:18558–61. [PubMed: 15792954]
12. Elrod JW, Wong R, Mishra S, Vagnozzi RJ, Sakthievel B, Goonasekera SA, Karch J, Gabel S, Farber J, Force T, Brown JH, Murphy E, Molkentin JD. Cyclophilin D controls mitochondrial pore-dependent Ca(2+) exchange, metabolic flexibility, and propensity for heart failure in mice. The Journal of clinical investigation. 2010; 120:3680–7. [PubMed: 20890047]
13. Menazza S, Wong R, Nguyen T, Wang G, Gucek M, Murphy E. CypD(−/−) hearts have altered levels of proteins involved in Krebs cycle, branch chain amino acid degradation and pyruvate metabolism. Journal of molecular and cellular cardiology. 2013; 56:81–90. [PubMed: 23262437]
14. Krump-Konvalinkova V, Bittinger F, Unger RE, Peters K, Lehr HA, Kirkpatrick CJ. Generation of human pulmonary microvascular endothelial cell lines. Laboratory investigation; a journal of technical methods and pathology. 2001; 81:1717–27.
15. Palmer AE, Tsien RY. Measuring calcium signaling using genetically targetable fluorescent indicators. Nature protocols. 2006; 1:1057–65.
16. Marcu R, Neeley CK, Karamanlidis G, Hawkins BJ. Multi-parameter measurement of the permeability transition pore opening in isolated mouse heart mitochondria. Journal of visualized experiments: JoVE. 2012
17. Hung YP, Albeck JG, Tantama M, Yellen G. Imaging cytosolic NADH-NAD(+) redox state with a genetically encoded fluorescent biosensor. Cell Metab. 2011; 14:545–54. [PubMed: 21982714]
18. Williamson DH, Lund P, Krebs HA. The redox state of free nicotinamide-adenine dinucleotide in the cytoplasm and mitochondria of rat liver. The Biochemical journal. 1967; 103:514–27. [PubMed: 4291787]
19. Baker M, Robinson SD, Lechertier T, Barber PR, Tavora B, D'Amico G, Jones DT, Vojnovic B, Hodivala-Dilke K. Use of the mouse aortic ring assay to study angiogenesis. Nature protocols. 2012; 7:89–104.
20. Jung Y, Dziennis S, Zhi Z, Reif R, Zheng Y, Wang RK. Tracking dynamic microvascular changes during healing after complete biopsy punch on the mouse pinna using optical microangiography. PloS one. 2013; 8:e57976. [PubMed: 23469122]

21. Denton RM, McCormack JG. The calcium sensitive dehydrogenases of vertebrate mitochondria. Cell calcium. 1986; 7:377–86. [PubMed: 3545489]
22. Marcu R, Wiczer BM, Neeley CK, Hawkins BJ. Mitochondrial Matrix Ca2+ Accumulation Regulates Cytosolic NAD+/NADH Metabolism, Protein Acetylation and Sirtuins Expression. Molecular and cellular biology. 2014; 15:2890–2902. [PubMed: 24865966]
23. Di Lisa F, Ziegler M. Pathophysiological relevance of mitochondria in NAD(+) metabolism. FEBS Lett. 2001; 492:4–8. [PubMed: 11248227]
24. Houtkooper RH, Pirinen E, Auwerx J. Sirtuins as regulators of metabolism and healthspan. Nat Rev Mol Cell Biol. 2012; 13:225–38. [PubMed: 22395773]
25. Zhang Q, Wang SY, Fleuriel C, Leprince D, Rocheleau JV, Piston DW, Goodman RH. Metabolic regulation of SIRT1 transcription via a HIC1:CtBP corepressor complex. Proc Natl Acad Sci U S A. 2007; 104:829–33. [PubMed: 17213307]
26. Palty R, Silverman WF, Hershfinkel M, Caporale T, Sensi SL, Parnis J, Nolte C, Fishman D, Shoshan-Barmatz V, Herrmann S, Khananshvili D, Sekler I. NCLX is an essential component of mitochondrial Na+/Ca2+ exchange. Proceedings of the National Academy of Sciences of the United States of America. 2010; 107:436–41. [PubMed: 20018762]
27. Ogryzko VV, Schiltz RL, Russanova V, Howard BH, Nakatani Y. The transcriptional coactivators p300 and CBP are histone acetyltransferases. Cell. 1996; 87:953–9. [PubMed: 8945521]
28. Zhang Q, Wang SY, Fleuriel C, Leprince D, Rocheleau JV, Piston DW, Goodman RH. Metabolic regulation of SIRT1 transcription via a HIC1:CtBP corepressor complex. Proceedings of the National Academy of Sciences of the United States of America. 2007; 104:829–33. [PubMed: 17213307]
29. Hamada K, Sasaki T, Koni PA, Natsui M, Kishimoto H, Sasaki J, Yajima N, Horie Y, Hasegawa G, Naito M, Miyazaki J, Suda T, Itoh H, Nakao K, Mak TW, Nakano T, Suzuki A. The PTEN/PI3K pathway governs normal vascular development and tumor angiogenesis. Genes & development. 2005; 19:2054–65. [PubMed: 16107612]
30. Song P, Wu Y, Xu J, Xie Z, Dong Y, Zhang M, Zou MH. Reactive nitrogen species induced by hyperglycemia suppresses Akt signaling and triggers apoptosis by upregulating phosphatase PTEN (phosphatase and tensin homologue deleted on chromosome 10) in an LKB1-dependent manner. Circulation. 2007; 116:1585–95. [PubMed: 17875968]
31. Ikenoue T, Inoki K, Zhao B, Guan KL. PTEN acetylation modulates its interaction with PDZ domain. Cancer Res. 2008; 68:6908–12. [PubMed: 18757404]
32. Di Lorenzo A, Fernandez-Hernando C, Cirino G, Sessa WC. Akt1 is critical for acute inflammation and histamine-mediated vascular leakage. Proc Natl Acad Sci U S A. 2009; 106:14552–7. [PubMed: 19622728]
33. Abid MR, Guo S, Minami T, Spokes KC, Ueki K, Skurk C, Walsh K, Aird WC. Vascular endothelial growth factor activates PI3K/Akt/forkhead signaling in endothelial cells. Arterioscler Thromb Vasc Biol. 2004; 24:294–300. [PubMed: 14656735]
34. Ramaswamy S, Nakamura N, Vazquez F, Batt DB, Perera S, Roberts TM, Sellers WR. Regulation of G1 progression by the PTEN tumor suppressor protein is linked to inhibition of the phosphatidylinositol 3-kinase/Akt pathway. Proceedings of the National Academy of Sciences of the United States of America. 1999; 96:2110–5. [PubMed: 10051603]
35. Tavecchio M, Lisanti S, Lam A, Ghosh JC, Martin NM, O'Connell M, Weeraratna AT, Kossenkov AV, Showe LC, Altieri DC. Cyclophilin D extramitochondrial signaling controls cell cycle progression and chemokine-directed cell motility. The Journal of biological chemistry. 2013; 288:5553–61. [PubMed: 23303179]
36. Nakagawa T, Shimizu S, Watanabe T, Yamaguchi O, Otsu K, Yamagata H, Inohara H, Kubo T, Tsujimoto Y. Cyclophilin D-dependent mitochondrial permeability transition regulates some necrotic but not apoptotic cell death. Nature. 2005; 434:652–8. [PubMed: 15800626]
37. Barsukova A, Komarov A, Hajnoczky G, Bernardi P, Bourdette D, Forte M. Activation of the mitochondrial permeability transition pore modulates Ca2+ responses to physiological stimuli in adult neurons. The European journal of neuroscience. 2011; 33:831–42. [PubMed: 21255127]

38. Hopper RK, Carroll S, Aponte AM, Johnson DT, French S, Shen RF, Witzmann FA, Harris RA, Balaban RS. Mitochondrial matrix phosphoproteome: effect of extra mitochondrial calcium. Biochemistry. 2006; 45:2524–36. [PubMed: 16489745]

39. Karamanlidis G, Lee CF, Garcia-Menendez L, Kolwicz SC Jr, Suthammarak W, Gong G, Sedensky MM, Morgan PG, Wang W, Tian R. Mitochondrial complex I deficiency increases protein acetylation and accelerates heart failure. Cell Metab. 2013; 18:239–50. [PubMed: 23931755]

40. Kunz WS, Davis EJ. Control of reversible intracellular transfer of reducing potential. Archives of biochemistry and biophysics. 1991; 284:40–6. [PubMed: 1824912]

41. Orimo M, Minamino T, Miyauchi H, Tateno K, Okada S, Moriya J, Komuro I. Protective role of SIRT1 in diabetic vascular dysfunction. Arteriosclerosis, thrombosis, and vascular biology. 2009; 29:889–94.

42. Rajendrasozhan S, Yang SR, Kinnula VL, Rahman I. SIRT1, an antiinflammatory and antiaging protein, is decreased in lungs of patients with chronic obstructive pulmonary disease. American journal of respiratory and critical care medicine. 2008; 177:861–70. [PubMed: 18174544]

43. Gerhart-Hines Z, Rodgers JT, Bare O, Lerin C, Kim SH, Mostoslavsky R, Alt FW, Wu Z, Puigserver P. Metabolic control of muscle mitochondrial function and fatty acid oxidation through SIRT1/PGC-1alpha. The EMBO journal. 2007; 26:1913–23. [PubMed: 17347648]

44. Onishi A, Miyamae M, Kaneda K, Kotani J, Figueredo VM. Direct evidence for inhibition of mitochondrial permeability transition pore opening by sevoflurane preconditioning in cardiomyocytes: comparison with cyclosporine A. Eur J Pharmacol. 2012; 675:40–6. [PubMed: 22166375]

45. Sundaresan NR, Pillai VB, Wolfgeher D, Samant S, Vasudevan P, Parekh V, Raghuraman H, Cunningham JM, Gupta M, Gupta MP. The deacetylase SIRT1 promotes membrane localization and activation of Akt and PDK1 during tumorigenesis and cardiac hypertrophy. Sci Signal. 2011; 4:ra46. [PubMed: 21775285]

46. Wang H, Liu H, Chen K, Xiao J, He K, Zhang J, Xiang G. SIRT1 promotes tumorigenesis of hepatocellular carcinoma through PI3K/PTEN/AKT signaling. Oncology reports. 2012; 28:311–8. [PubMed: 22552445]

47. Lee SR, Yang KS, Kwon J, Lee C, Jeong W, Rhee SG. Reversible inactivation of the tumor suppressor PTEN by H2O2. The Journal of biological chemistry. 2002; 277:20336–42. [PubMed: 11916965]

48. Stein S, Matter CM. Protective roles of SIRT1 in atherosclerosis. Cell Cycle. 2011; 10:640–7. [PubMed: 21293192]

49. Potente M, Ghaeni L, Baldessari D, Mostoslavsky R, Rossig L, Dequiedt F, Haendeler J, Mione M, Dejana E, Alt FW, Zeiher AM, Dimmeler S. SIRT1 controls endothelial angiogenic functions during vascular growth. Genes & development. 2007; 21:2644–58. [PubMed: 17938244]

Novelty & Significance

What Is Known?

- Vascular endothelial cells regulate blood vessel function and endothelial dysfunction contributes to cardiovascular disease.
- Endothelial cells contain functional mitochondria but rely primarily on cytosolic glucose metabolism for their energetic requirements.
- Endothelial mitochondria can generate and release reactive oxygen species to initiate intracellular signaling.

What New Information Does This Article Contribute?

- In endothelial cells, the mitochondrial permeability transition pore (mPTP) plays an important physiological role in matrix calcium homeostasis and NAD^+/NADH metabolism.
- Genetic inactivation of mPTP by deletion of Cyclophilin D led to an imbalance in NAD^+/NADH metabolism, which was transmitted to the nucleus to regulate gene expression independent of reactive oxygen species.
- Endothelial cells and mice deficient in Cyclophilin D exhibit constitutive activation of pro-angiogenic Akt that enhances vessel formation in response to wounding.

Vascular endothelial cells (ECs) are critical for normal blood vessel function but their dysfunction also contribute to cardiovascular disease, diabetes, aging, and cancer. A common characteristic of dysfunctional ECs is excessive generation of mitochondrial reactive oxygen species and impaired vessel growth (angiogenesis). In the present study we examined the signaling pathways by which endothelial cell mitochondria impact angiogenesis. We found that genetic deletion of Cyclophilin D (CypD) inactivated the mitochondrial permeability transition pore (mPTP) and triggered a constitutive increase in mitochondrial calcium levels and NADH generation. As a result, CypD-deficient ECs and mice exhibited an imbalance in NAD^+/NADH metabolism that influenced the expression of the NAD^+-dependent deacetylase SIRT1 and the angiogenic molecule PTEN. These genetic changes led to the constitutive activation of Akt, resulting in enhanced angiogenesis both in vitro and in vivo. These results elucidate a novel link between mitochondrial bioenergetics and the regulation of gene expression, and highlight the importance of mitochondrial metabolism in modulating endothelial-mediated vessel formation.

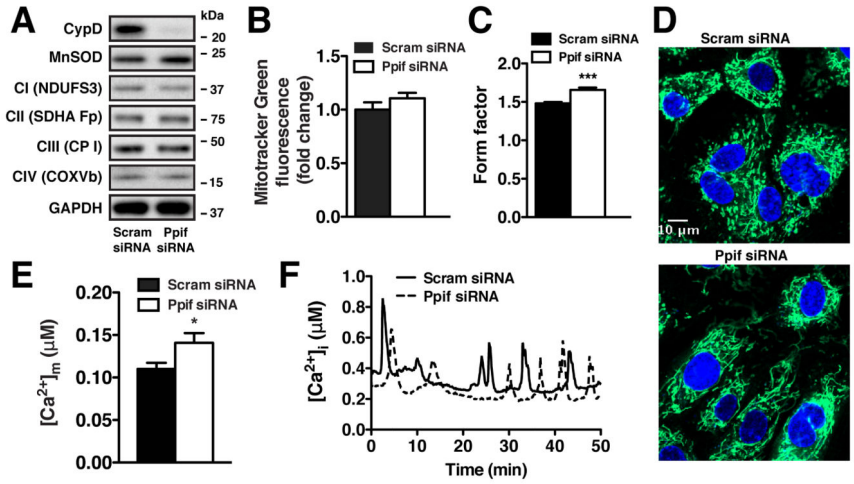

Figure 1. CypD knockdown increases $[Ca^{2+}]_m$ in ECs

(A) Representative immunoblot of CypD and mitochondrial proteins MnSOD, NADH dehydrogenase iron-sulfur protein 3 (NDUFS3), Succinate dehydrogenase flavoprotein subunit (SDHA Fp), Ubiquinol-Cytochrome c reductase core protein I (CP I), Cytochrome c oxidase subunit Vb (COXVb) in HPAECs transfected with scrambled or Ppif siRNA, normalized to GAPDH. (B) FACS measurement of cellular mitochondrial content using MitoTracker Green (50 nmol/L) (mean ± SEM, n=3). (C) Form factor quantification of mitochondrial morphology for scrambled (n=189) and Ppif (n=137) siRNA HPAECs (mean ± SEM). (D) Representative confocal images of mitochondrial morphology in scrambled and Ppif siRNA HPAECs stained with MitoTracker Green (50 nmol/L) and Hoechst 33342 (10 μg/ml). (E) Mean calibrated basal $[Ca^{2+}]_m$ concentration of scrambled (n=137) and Ppif (n=12) siRNA HPAECs measured with Cameleon D3cpv sensor. (F) Microscopic analysis of intracellular Ca^{2+} concentration measured with Fura-2 AM in scrambled and Ppif siRNA HPAECs in the presence of 5% FBS.

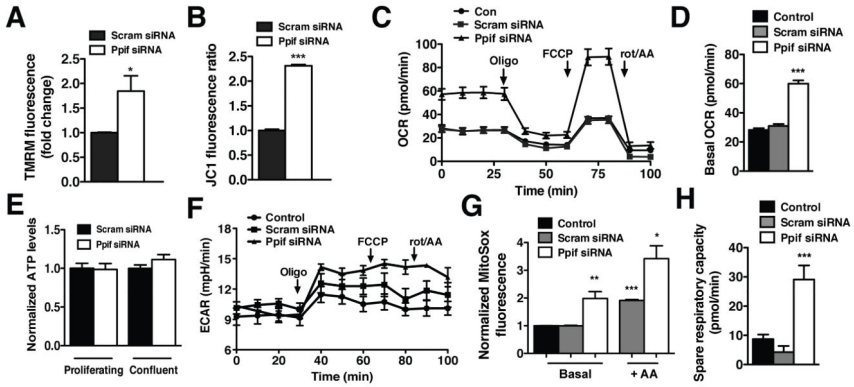

Figure 2. CypD regulates endothelial mitochondrial function

FACS measurement of mitochondrial membrane potential in scrambled and Ppif siRNA HPAECs stained with (A) TMRM (30 nmol/L) and (B) JC-1 (0.5 μg/μl) (mean ± SEM, n=3). (C) OCR of control, scrambled siRNA and Ppif siRNA HPAECs upon addition of oligomycin (1 μmol/L), FCCP (1 μmol/L), rotenone and antimycin (1 μmol/L) measured with Seahorse XF24 analyzer. (D) Quantification of basal OCR of control, scrambled siRNA and Ppif siRNA HPAECs (mean ± SEM, n=3). (E) Normalized baseline ATP content of scrambled and Ppif siRNA HPAECs in proliferating and confluent cultures (mean ± SEM, n=3). (F) Seahorse X24 ECAR measurement of control, scrambled siRNA and Ppif siRNA HPAECs upon addition of oligomycin (1 μmol/L), FCCP (1 μmol/L), rotenone and antimycin A (1 μmol/L). (G) FACS measurement of mitochondrial superoxide production using MitoSOX Red (5 μmol/L) in control, scrambled siRNA and Ppif siRNA HPAECs at baseline and after antimycin A (5 μmol/L) (mean ± SEM, n=3). (H) Quantification of spare respiratory capacity of control, scramble siRNA and Ppif siRNA HPAECs (mean ± SEM, n=3).

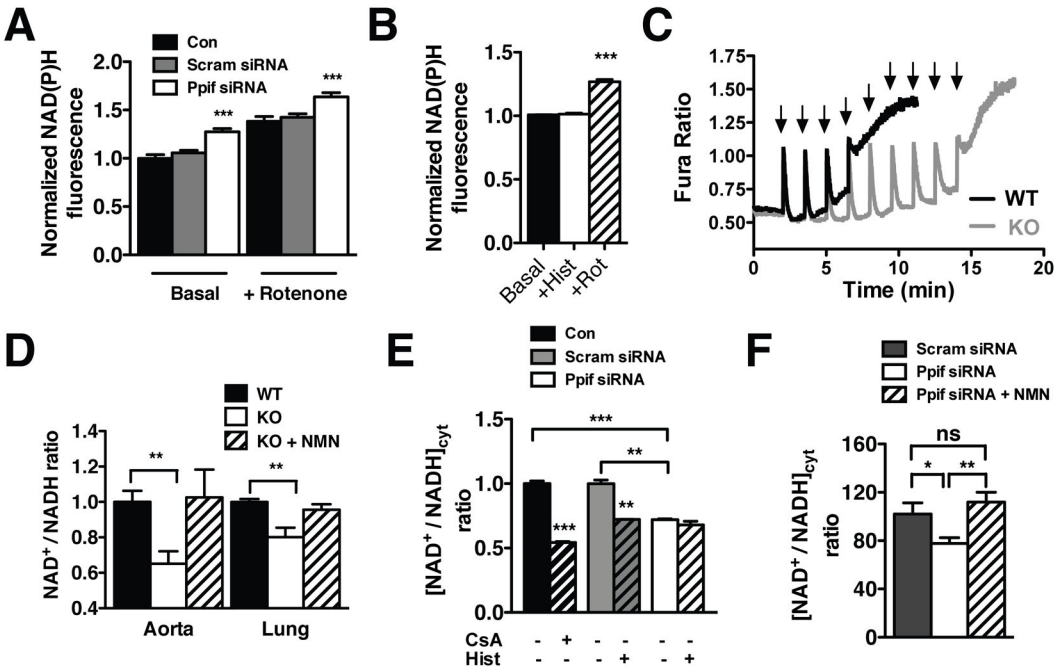

Figure 3. Genetic targeting of CypD influences cellular NAD$^+$/NADH homeostasis

(A) Fluorescence microscopy measurement of mitochondrial NAD(P)H autofluorescence in control (n=106), scrambled siRNA (n=215) and Ppif siRNA (n=195) HPAECs at baseline and upon rotenone (5 μM) (mean ± SEM). (B) Normalized mitochondrial NAD(P)H autofluorescence in Ppif siRNA HPAECs at baseline and upon histamine (100 nmol/L) and rotenone (5 μmol/L) (mean ± SEM, n=27). (C) Spectrofluorometric measurement of calcium retention capacity of WT and CypD KO liver mitochondria (1 mg/ml, 2 mmol/L succinate, 20 μmol/L $CaCl_2$ pulses every 1.5 min) using Fura-FF as an indicator of extramitochondrial Ca^{2+}. (D) Total intracellular NAD$^+$/NADH ratio of aorta and lung tissues from WT and CypD KO mice ± NMN (100 mg/kg, 1hr) normalized to the WT mice ratio values (mean ± SEM, n=6 mice/group). (E) Cytosolic NAD$^+$/NADH ratio calculated from the measured lactate/pyruvate ratio of control, scrambled siRNA and Ppif siRNA HPAECs at baseline and control cells treated with CsA (1 μmol/L) and histamine (100 nmol/L) (mean ± SEM, n=3). (F) Cytosolic NAD$^+$/NADH ratio in scrambled (n=72), Ppif siRNA (n=65) and NMN (100 μmol/L) treated Ppif siRNA (n=19) HPAECs calculated from the Peredox green-to-red fluorescence ratio after sensor calibration (mean ± SEM).

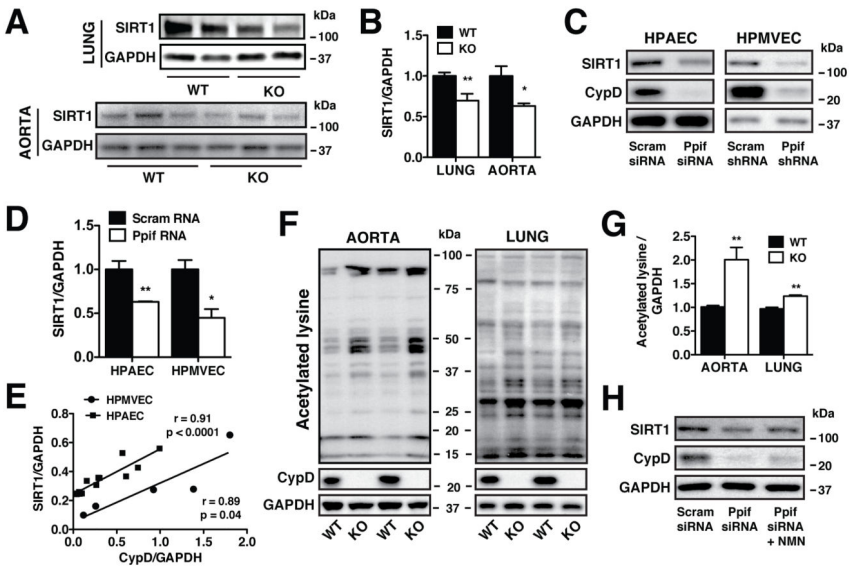

Figure 4. CypD-mediated [NAD^+/NADH]$_{cyt}$ alterations influence SIRT1 expression

(A), (B) Western blot analysis and densitometry quantification of SIRT1 expression in lung and aorta extracts from WT and CypD KO mice (mean ± SEM, n=8 mice/group lung, n=5 mice/group aorta) normalized to GAPDH. (C), (D) Western blot analysis and densitometry quantification of SIRT1 expression in HPAECs (n=6) and HPMVECs (n=3) in which CypD was genetically targeted using siRNA and shRNA normalized to GAPDH (mean ± SEM). (E) Correlation between CypD and SIRT1 expression in HPAECs (squares, n=13) and HPMVECs (circles, n=5). Values represent expression normalized to GAPDH and points represent individual experiments. (F), (G) Western blot analysis and densitometry quantification of aorta and lung extracts from WT and CypD KO mice probed with a pan-Acetylated lysine antibody and normalized to GAPDH (mean ± SEM, n=6 mice/group aorta, n=3 mice/group lung). (H) Western blot analysis of SIRT1 levels in Ppif siRNA HPAECs treated with NMN (100 μmol/L, 48 hr) normalized to GAPDH.

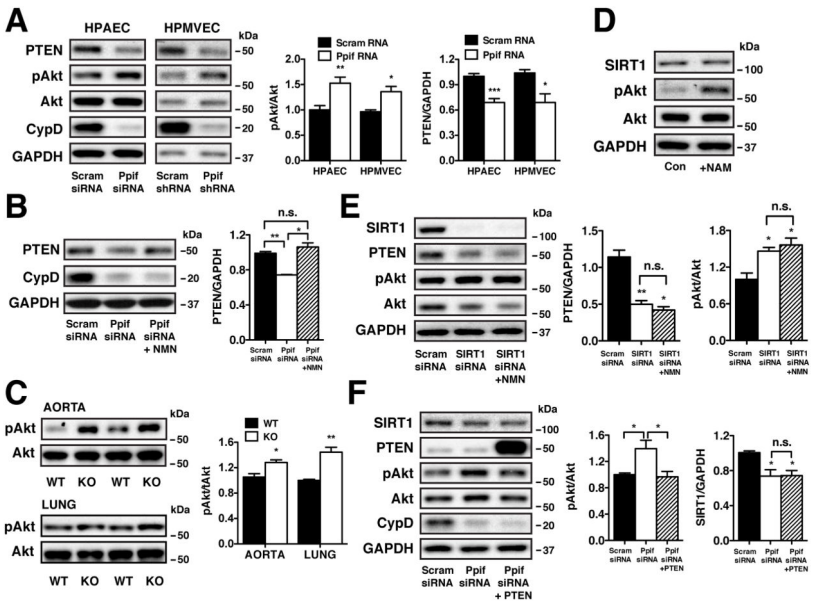

Figure 5. CypD-mediated SIRT1 alterations influence PTEN expression and Akt phosphorylation

(A) Western blot analysis and densitometry quantification of PTEN and pAkt(Ser^{473}) expression in scrambled and Ppif siRNA HPAECs (n=6) and scrambled and Ppif shRNA HPMVECs (n=3) normalized to total Akt and GAPDH (mean ± SEM). (B) Western blot analysis and densitometry quantification of PTEN expression in Ppif siRNA HPAECs ± NMN (100 μmol/L, 48 hr) normalized to GAPDH (mean ± SEM, n=3). (C) Western blot analysis and densitometry quantification of pAkt(Ser^{473}) expression in aorta and lung from WT and CypD KO mice normalized to total Akt (mean ± SEM, n=3). (D) Western blot analysis of SIRT1 and pAkt(Ser^{473}) levels in control and NAM (5 mmol/L) + TSA (500 nmol/L) treated HPAECs (24h) normalized to GAPDH and total Akt. (E) Western blot analysis and densitometry quantification of PTEN and pAkt(Ser^{473}) levels in HPAECs expressing scrambled siRNA and SIRT1 siRNA ± NMN (100 μmol/L, 48 h) normalized to GAPDH and total Akt (mean ± SEM, n=3). (F) Western blot analysis and densitometry quantification of SIRT1, PTEN and pAkt(Ser^{473}) levels in scrambled and Ppif siRNA HPAECs expressing the empty vector PSG5L and Ppif siRNA HPAECs expressing PSG5L PTEN, normalized to GAPDH (mean ± SEM, n=3).

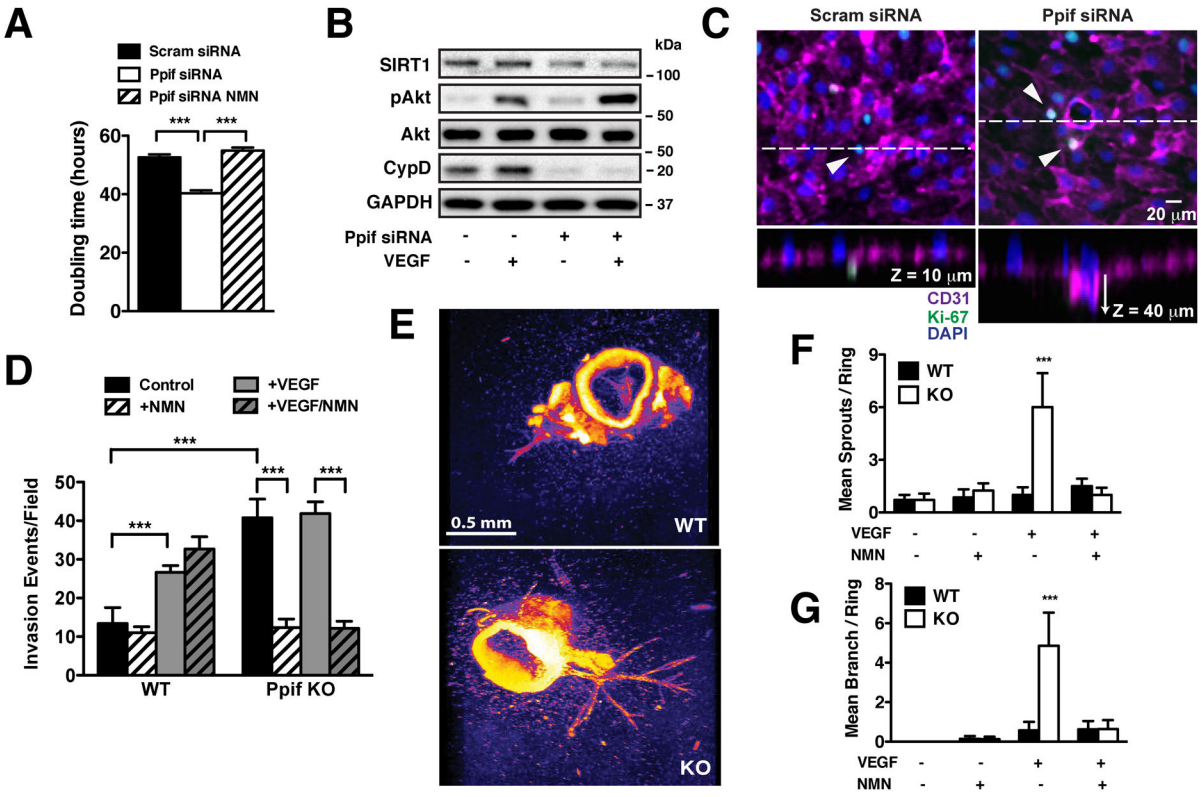

Figure 6. CypD deletion increases endothelial proliferation and angiogenesis

(A) Doubling time of scrambled and Ppif siRNA HPAECs ± NMN (100 μmol/L, 48 hr) (mean ± SEM, n=3). (B) Western blot analysis of SIRT1 and pAkt(Ser^{473}) expression in serum-starved scrambled and Ppif siRNA HPAECs ± VEGF (50 ng/ml, 15 min) normalized to GAPDH and total Akt. (C) Representative confocal images of scrambled and Ppif siRNA HPAECs + VEGF (50 ng/ml) invading on collagen matrix. Cells were stained for endothelial marker CD31 (magenta), proliferation marker Ki-67 (green) and nuclei with DAPI (blue). (D) Quantification of invasion events for scrambled and Ppif siRNA HPAECs at baseline and upon VEGF (50 ng/ml) ± NMN (100 μmol/L) (mean ± SEM, n=3). (E) Confocal images of angiogenic vessel growth in WT and CypD KO aortic rings after VEGF treatment (30 ng/ml), stained with DAPI. (F), (G) Quantitation of primary sprouts and secondary branches of WT and CypD KO aortic rings at baseline and upon VEGF (30 ng/ml) ± NMN (100 μmol/L) (mean ± SEM, n= 3).

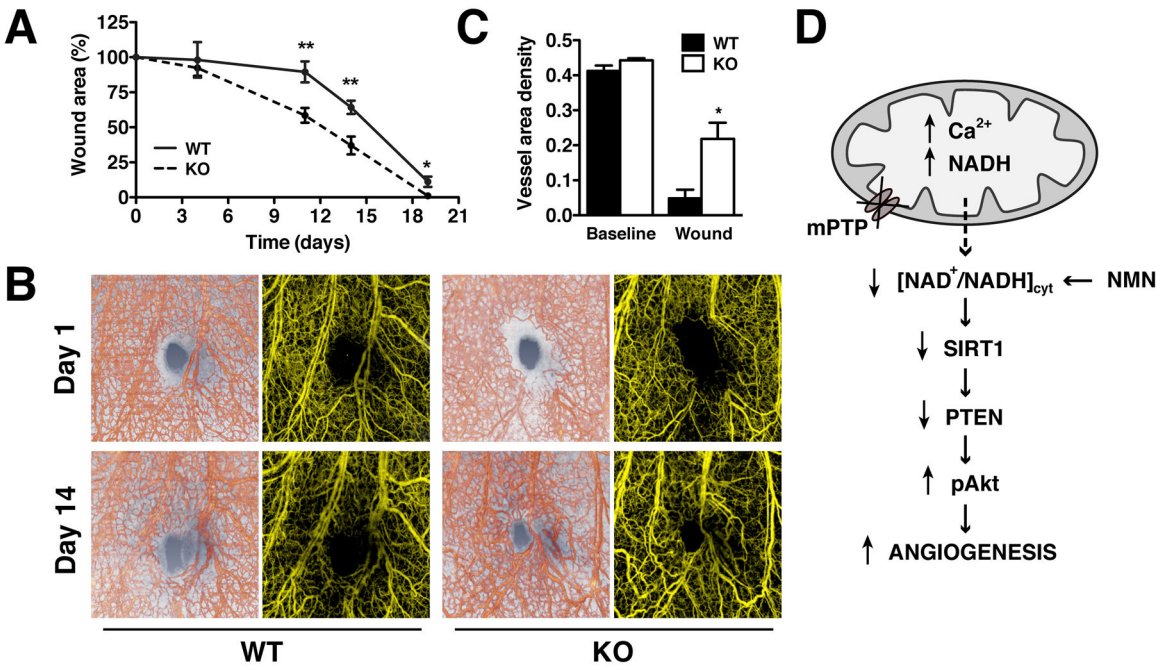

Figure 7. CypD knockdown accelerates wound healing and neovascularization in vivo

(A) Wound area progression in WT and CypD KO mice after skin excision of mouse pinnae with a biopsy punch. Measurements were normalized to the day 1 wound size (mean ± SEM, n=6/group). (B) Representative OMAG images of microvascular changes during wound healing in WT and CypD KO mice, at days 1 and 14 after wounding (structure images of pinna cross-section overlaid with 3D view of OMAG vasculature, red, and projection view images of OMAG vasculature, yellow). (C) Vessel area density in WT and CypD KO mice at baseline and wound location at 14 days post wounding calculated from projection OMAG images (mean ± SEM, n=3 mice/group). (D) Genetic or pharmacological inhibition of mPTP in ECs increases matrix Ca^{2+} and stimulates NADH accumulation. Simultaneously a decrease in cytosolic NAD^+/NADH ratio downregulates SIRT1 and PTEN resulting in Akt activation and increased angiogenesis. NMN supplementation restores NAD^+/NADH ratio and recovers the phenotype.